Bioorganic & Medicinal Chemistry 26 (2018) 5006–5017

Contents lists available at ScienceDirect

Bioorganic & Medicinal Chemistry

journal homepage: www.elsevier.com/locate/bmc

Discovery of a non-toxic [1,2,4]triazolo[1,5-*a*]pyrimidin-7-one (**WS-10**) that modulates ABCB1-mediated multidrug resistance (MDR)

Liming Chang[a,b,f,1], Mengwu Xiao[c,i,1], Linlin Yang[e], Shuai Wang[a,b,f], Sai-Qi Wang[a,b,f], Andreas Bender[c], Aixi Hu[i], Zhe-Sheng Chen[d], Bin Yu[a,b,f,g,h,*], Hong-Min Liu[a,b,f,*]

[a] School of Pharmaceutical Sciences, Zhengzhou University, Zhengzhou 450001, China
[b] Co-Innovation Center of Henan Province for New Drug R & D and Preclinical Safety, Zhengzhou 450001, China
[c] Centre for Molecular Informatics, Department of Chemistry, University of Cambridge, Lensfield Road, Cambridge CB2 1EW, UK
[d] College of Pharmacy and Health Sciences, St. John's University, Queens, NY 11439, USA
[e] Department of Pharmacology, School of Basic Medical Sciences, Zhengzhou University, Zhengzhou 450001, China
[f] Key Laboratory of Technology of Drug Preparation (Zhengzhou University), Ministry of Education of China, Zhengzhou 450001, China
[g] College of Chemistry and Molecular Engineering, Zhengzhou University, Zhengzhou 450001, China
[h] Guangdong Provincial Key Laboratory of New Drug Screening, Guangzhou 510033, China
[i] College of Chemistry and Chemical Engineering, Hunan University, Changsha 410082, China

ARTICLE INFO

Keywords:
Multidrug resistance (MDR)
ABC transporters
ABCB1
Triazolo [1,5-*a*]pyrimidin-7-one

ABSTRACT

Multidrug resistance (MDR) has been shown to reduce the effectiveness of chemotherapy. Strategies to overcoming MDR have been widely explored in the last decades, leading to a generation of numerous small molecules targeting ABC and MRP transporters. Among the ABC family, ABCB1 plays key roles in the development of drug resistance and is the most well studied. In this work, we report the discovery of a non-toxic [1,2,4]triazolo[1,5-*a*]pyrimidin-7-one (**WS-10**) from our structurally diverse in-house compound collection that selectively modulates ABCB1-mediated multidrug resistance. **WS-10** enhanced the intracellular accumulation of paclitaxel in SW620/Ad300 cells, but did not affect the expression of ABCB1 Protein and ABCB1 localization. The cellular thermal shift assay (CETSA) showed that **WS-10** was able to bind to ABCB1, which could be responsible for the reversal effect of **WS-10** toward paclitaxel and doxorubicin in SW620/Ad300 cells. Docking simulations were performed to show the possible binding modes of **WS-10** within ABCB1 transporter. To conclude, **WS-10** could be used as a template for designing new ABCB1 modulators to overcome ABCB1-mediated multidrug resistance.

1. Introduction

There are many chemotherapeutic agents used as first-line anticancer drugs, such as paclitaxel and doxorubicin.[1] However, the multidrug resistance (MDR) arising during chemotherapy could result in tumor recurrence and metastasis.[2,3] Overexpression of the ATP-Binding Cassette (ABC) transporters could be responsible for the MDR.[4] The ABC transporters utilize the energy generated by ATP hydrolysis to transport various substrates across cellular membranes, therefore leading to elevated drug efflux in cancer cells.[5,6] The most well studied ABC transporter in humans is ABCB1 (also known as P-gp/MDR1), which has been found to be essential in mediating the efflux of chemotherapeutic drugs like paclitaxel.[7,8]

It is believed that the inhibitors of transporters which either decrease the expression of ABC proteins or inhibit the efflux function of ABC transporters could enhance chemosensitivity toward multidrug resistant cancer cells.[9] Although numerous inhibitors of ABCB1 have been identified,[10–16] most of them such as some kinase inhibitors are cytotoxic. Therefore, the identification of non-toxic ABCB1 modulators is still urgently needed.[10,17] Following our previous work on the identification of ABCB1 inhibitors,[18] we herein report the discovery of a non-toxic compound from our in-house molecular library, **WS-10**, which is able to modulate ABCB1-mediated multidrug resistance (MDR). **WS-10** could hence be used as a new template to develop non-toxic ABCB1 modulators.

* Corresponding authors.
E-mail addresses: zzuyubin@hotmail.com (B. Yu), liuhm@zzu.edu.cn (H.-M. Liu).
[1] These two authors contributed equally to this work.

https://doi.org/10.1016/j.bmc.2018.08.021
Received 3 April 2018; Received in revised form 25 July 2018; Accepted 16 August 2018
Available online 18 August 2018
0968-0896/

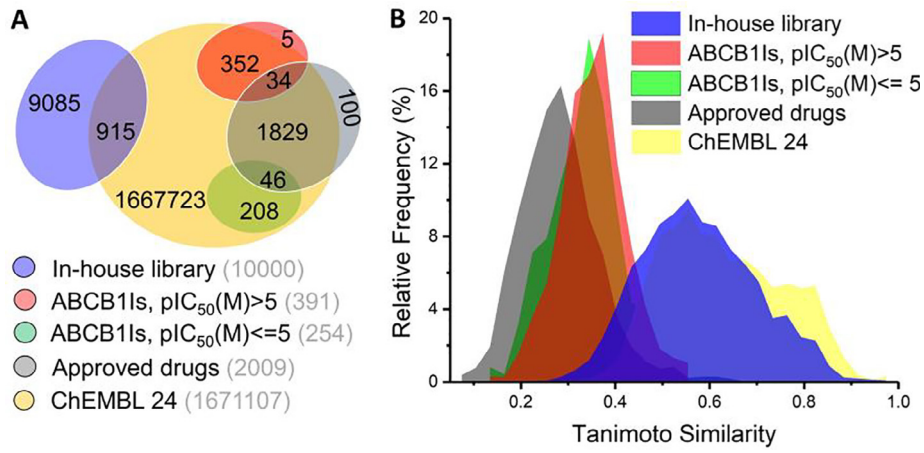

Fig. 1. (A) Venn diagram showing the intersection among ABCB1 inhibitors, approved drugs, ChEMBL and our in-house library. (B) Distribution of the maximum pairwise Tanimoto similarity of Morgan fingerprint between each compound in our in-house library and all compounds in other libraries. Intra-group similarity of in-house library (blue). The structural similarity between the in-house library and approved drugs (gray), ABCB1 inhibitors (pIC_{50} (M) > 5: red; pIC_{50} (M) ≤5: green), ChEMBL 24 (yellow). (For interpretation of the references to color in this figure legend, the reader is referred to the web version of this article.)

2. Results and discussion

2.1. Chemical space analysis of our in-house library

The in-house screening collection utilized in this work includes about 10,000 compounds selected from multiple commercial vendors based upon in-house developed filters for lead-like molecules, as well as compounds synthesized in the lab from Zhengzhou University. Cheminformatics approaches were applied to provide complementary information on our in-house compound screening library, enabling identification of unexplored regions of chemical space with potential biological relevance.

2.1.1. Compound library intersection and similarity analysis

The structure overlap among our in-house compound library and other compound libraries were analyzed (Fig. 1A), showing that our compound set does not overlap with current reported ABCB1 inhibitors (ABCB1Is) in ChEMBL and approved drugs, while about 9% (915 compounds) of our in-house compounds were present in the ChEMBL database. It can be seen in Fig. 1B that our in-house library is more structurally similar to ABCB1 inhibitors than approved drugs. Furthermore, the intra-group of the in-house compound set is relatively high because some compounds are synthesized by similar synthetic routes and starting materials.

2.1.2. Structure and physicochemical properties analysis

(1) Exploratory data analysis

The quality of a compound collection can be defined in many different ways but very often, physicochemical properties and the presence of some unwanted chemical groups are used in the field at the beginning of the project. We found that 97.1% of the compounds in the in-house library displayed drug-like properties according to Lipinski's rule of five.[19] On the other hand, 98.3% of the compounds are within the Veber rule's boundaries,[20] which indicates a high probability of good oral bioavailability. And more importantly, as shown in the distribution analysis of physicochemical properties (Fig. 2a–f), our compound set has similar property distribution with both ABCB1 inhibitors and approved drugs, but the values of XLOGP3, Molecular Weight (MW), Number of Rotatable Bonds (nRotB), and Topological Polar Surface (TPSA) of both ABCB1 inhibitors and in-house library are relatively higher than those of approved drugs; And our compound set is more similar to ABCB1 inhibitors than approved drugs in terms of this feature. The compound **WS-10** identified from the in-house library also has drug-like properties: MW = 374.09, XLOGP3 = 3.65, Number of H-Bond Donor (nHBDon) = 2, Number of H-Bond Acceptor (nHBAcc) = 7, nRotB = 4, TPSA = 113.79 $Å^2$.

(2) Chemical space analysis

Chemical space can be visualized as 2D/3D scatter plot in which distances between data points correspond to their structural or physicochemical similarities. Here two types of descriptors were used: physicochemical properties and Morgan fingerprints.[21] Physicochemical property analysis (Fig. 3A) shows that the in-house compound library has a relatively concentrated drug-like physicochemical property space (the XLOGP3 and MW values of in-house compounds within the 95% confidence ellipse are in the range of about 0–7 and 250–550, respectively) and composites a special subset of approved drugs and published active ABCB1 inhibitors. Another interesting point is that ABCB1 inhibitors and our in-house compounds tend to be more hydrophobic and have a bigger molecular weight (Fig. 3A), which were able to bind to the hydrophobic pockets of ABCB1 protein.

What can be seen in structural space (Fig. 3B) is that the structure diversity of the library employed in this work is significantly larger than those of both approved drugs and reported ABCB1 inhibitors. Additionally the structure–property space of inactive (pIC_{50} (M) ≤5) and active (pIC_{50} (M) > 5) ABCB1 inhibitors are partially overlapping (Fig. 3C, D); However, the majority of very active ABCB1 inhibitors (with higher pIC_{50} values, displayed in red) are located in a relatively distinct, and more hydrophobic chemical space. Therefore, improving the lipophilicity of **WS-10** (XLOGP3 = 3.65) may be a potential way for the optimization.

(3) Chemical fragment space

"Fragment Space" is smaller than "Chemical Space" and can be more effectively probed with a relatively small library. Analysis of scaffolds provides an opportunity to identify gaps in current libraries. Comparing to ChEMBL (1671107 compounds), our in-house library (10000 compounds) has excellent fragment diversity, including 412 (4857, ChEMBL) aromatic rings, 2527 (98074) unique ring systems, 7740 (497509) Bemis-Murcko frameworks,[22] 5994 (194519) Murcko generic scaffolds, 6511 (445009) RECAP fragments,[23] 3954 (285748) BRICS fragments.[24] Here we analyzed in more detail the difference of fragment space between active (pIC_{50} (M) > 5) and inactive (pIC_{50} (M) ≤5) ABCB1 inhibitors (Table 1). RECAP analysis shows that polymethoxy phenyl containing fragments, especially the 3,4,5-trimethoxy phenyl containing fragments, with significant higher relative frequency (0.64–2.43%) in active ABCB1 inhibitors comparing to the figure of the inactive (below 0.1%). Murcko scaffold analysis shows that Flavonoid/Flavan (3.07%) may be a good scaffold of ABCB1 inhibitors. And we also found that 2/3-membered fused ring systems, linked to another rings by 2–4 bond-length linkers, is a most common scaffold pattern in this table. These linkers include ester, acrylate, acrylamide group and butyl. **WS-10** (Scheme 1) also contains similar scaffold pattern with a 2-

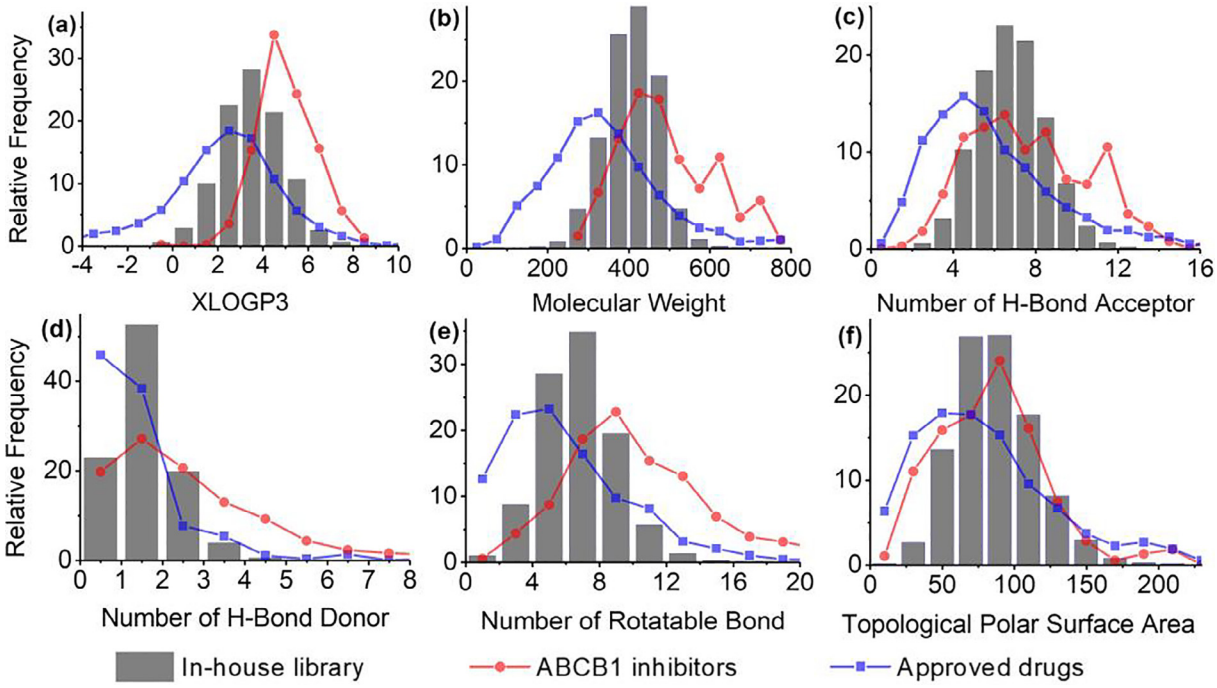

Fig. 2. Distributions of the molecular descriptors for in-house compounds (gray bars), ABCB1 inhibitors (pIC_{50} (M) > 5: red line) and approved drugs (blue line). (For interpretation of the references to color in this figure legend, the reader is referred to the web version of this article.)

membered fused ring ([1,2,4]-triazolo[1,5-*a*]pyrimidin-7-one) linked to another 2-membered fused ring (1*H*-benzo[*d*]imidazole) though 2-bond-length linker (—S—CH_2—). These fragments may provide useful structural information for further design of ABCB1 inhibitors.

2.2. Chemistry

WS-10 (also known as compound **4**) identified from our in-house molecular library was resynthesized according to our previously reported methods (Scheme 1).[25] Treatment of 3-amino-5-mercapto-1,2,4-triazole (**2**) with 2-chloromethylbenzimidazole (**2**) in acetone in the presence of Na_2CO_3 resulted in compound **3**, which then reacted with ethyl 3-oxo-3-phenylpropanoate in acetic acid under reflux, producing compound **4** in an overall yield of 21% within two steps.

2.3. *WS-10* exerted reversal effect on MDR cells overexpressing ABCB1

To select the non-toxic concentration of **WS-10**, the MTT assays against human colon cancer cell line SW620 and the doxorubicin-resistant ABCB1 overexpressed SW620/Ad300 cells were carried out. The human colon carcinoma cell lines SW620 and SW620/Ad300 are believed to be excellent models and therefore widely used to investigate the reversible effects of small-molecule modulators. As shown in Fig. 4A, **WS-10** displayed weak inhibition against SW620 and SW620/Ad300 cells with the IC_{50} value of 85.96 and 106.39 μM, respectively. The cytotoxicity toward five other cancer cell lines was also investigated (Fig. 4B). The results showed that treatment with **WS-10** at both 10 and 20 μM did not cause remarkable inhibitory effect on these cell lines. Therefore, 10 and 20 μM of **WS-10** were used for our next experiments.

The reversal effect on MDR cells overexpressing ABCB1 was studied by cell survival assays in the presence and absence of **WS-10** using the parental SW620 cell line and drug-resistant SW620/Ad300 cell line. Verapamil, an ABCB1 inhibitor, was used as the control compound. As shown in Table 2, **WS-10** treatment did not exhibit reversal effect on the resistance to paclitaxel, doxorubicin, and cisplatin in SW620 cells, the IC_{50} values of anticancer agents (paclitaxel, doxorubicin, and Cisplatin) or in combination with WS-10 were almost equal to that of verapamil. However, **WS-10** concentration-dependently decreased resistance to paclitaxel and doxorubicin (DOX) in SW620/Ad300 cells. **WS-10** at 20 μM exerted similar reversible effect on the drug resistance with verapamil (4.0 μM) in SW620/Ad300 cells. Co-treatment of SW620/Ad300 cells with paclitaxel or doxorubicin and WS-10 (20 μM) caused remarkable cytotoxicity with the IC_{50} values less than 1.0 μM, showing the synergistic effect. However, **WS-10** (20 μM) and verapamil (4.0 μM) did not increase the cytotoxicity of Cisplatin toward SW620/Ad300 cells. The difference could be explained by the fact that paclitaxel and DOX are ABCB1 substrates, while Cisplatin is non-ABCB1 substrate.[26] This finding is consistent with previous report by Richardson *et al.*[27]

The SW620/Ad300 cells are resistant to some therapeutic agents through multiple mechanisms, not solely due to the overexpression of ABCB1. To further elucidate the mechanisms of **WS-10** that modulates the MDR of cancer cells, we used the ABCB1-tansfected HEK293T/ABCB1 cell line and its parental HEK293T/NC cell line to further evaluate the effect of **WS-10** on the cell viability using the verapamil as the control. As shown in Table 3, like verapamil, treatment of **WS-10** did not significantly improve the sensitivity to paclitaxel and Cisplatin in HEK293T/ABCB1 and HEK293T/NC cells, while **WS-10** concentration-dependently enhanced sensitivity of HEK293T/ABCB1 cells to DOX with an IC_{50} value of 0.29 μM (treated with DOX and 20 μM of **WS-10**), equal to that of the group treated with DOX and verapamil (4 μM). Similar reversible effects were also observed in the group treated with paclitaxel and **WS-10**. The data further confirm that DOX is an ABCB1 substrate and **WS-10** could increase sensitivity of HEK293T/ABCB1 to DOX and paclitaxel.

2.4. *WS-10* enhanced the intracellular accumulation of paclitaxel in SW620/Ad300 cell line

To investigate the reversal mechanism of **WS-10**, we studied the effect of **WS-10** on the intracellular accumulation of paclitaxel in ABCB1-overexpressed SW620/Ad300 cells by the UPLC (Ultra Performance Liquid Chromatography) (Fig. 5). The results showed that

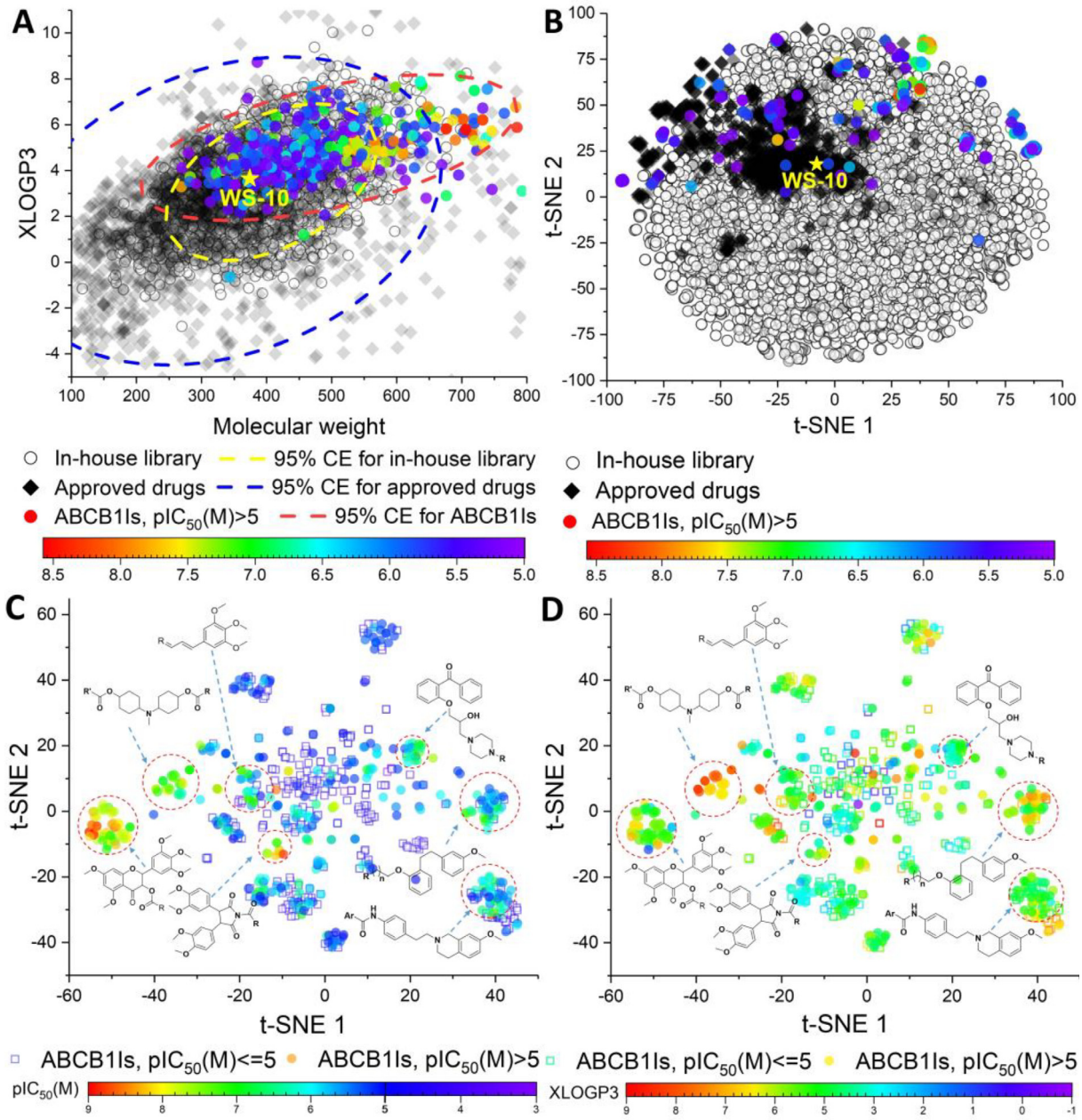

Fig. 3. Chemical space of the in-house library (black open circles), approved drugs (black filled diamond) and ABCB1 inhibitors (active: filled circles; inactive: open square; the color is based on the pIC_{50} (M) value of ABCB1 inhibitory activities). ABCB1Is: ABCB1 inhibitors; CE: confidence ellipse. (A) Molecular weight *versus* XLOGP3. (B-D) *t*-SNE plot using Morgan fingerprints (2048 bits). (For interpretation of the references to color in this figure legend, the reader is referred to the web version of this article.)

the intracellular accumulation of paclitaxel was significantly lower in the drug-resistant SW620/Ad300 cells than that in the parental SW620 cells. However, after treatment with **WS-10** at 10 and 20 μM for 72 h, the intracellular accumulation of paclitaxel significantly increased in the SW620/Ad300 cells. These results revealed that **WS-10** may increase the accumulation of paclitaxel possibly by inhibiting ABCB1.

2.5. Expression levels of several MDR-related proteins

To explore the potential mechanism of **WS-10**, we examined the expression levels of several MDR-related proteins in the SW620 and SW620/Ad300 cell lines, as well as HEK293T and its ABCB1-overexpressed cell line HEK293T/ABCB1. These MDR-related proteins include ABCB1, ABCG2, ABCC1, and ABCC10, which are implicated in the development of MDR in cancers. As depicted in Figs. 6 and 7, the expression levels of ABCB1 in both drug-resistant cell lines SW620/Ad300 and HEK293/ABCB1 changed significantly compared to their respective parental cell lines SW620 and HEK293/NC. The expression levels of ABCC10 also changed marginally in both drug-resistant cell lines. The results suggest that **WS-10** may alter the accumulation and efflux of chemotherapeutic agents by mainly modulating ABCB1.

2.6. The effect of *WS-10* on the expression levels of ABCB1 protein or the protein location of ABCB1

Drug-induced regulation of ABCB1 mRNA or protein can potentially affect the drug sensitivity of cancer cells to chemotherapeutics. Therefore, the expression level of ABCB1 protein was examined by the Western blot. As shown in Fig. 8, **WS-10** did not remarkably affect the expression of ABCB1 in SW620/Ad300 cells under different

Table 1
Fragments found in active and inactive ABCB1 inhibitors, with significant different relative frequency.

Fragment type	Structure	Relative frequency/count		Structure	Relative frequency/count	
		Active	Inactive		Active	Inactive
Murcko		3.07/12	0/0		1.28/5	0/0
Murcko generic		3.84/15	0/0	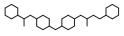	3.07/12	0/0
		2.30/9	0/0	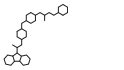	2.04/8	0/0
	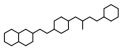	1.79/7	0/0	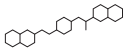	1.53/6	0/0
		1.28/5	0/0	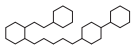	1.28/5	0/0
RECAP	 or 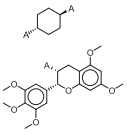	3.00/42	0/0		2.72/38	0.12/1
		2.43/34	0/0		2.17/29	0.12/1
	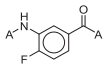	1.00/14	0/0	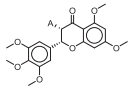	0.86/12	0/0
	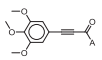	0.86/12	0/0		0.86/12	0/0
	 or	0.86/12	0/0		0.64/9	0/0
		0.57/8	0/0		0.36/7	0/0
Aromatic Ring		1.36/7	0/0	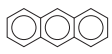	0.78/4	0/0
Links		10.18/57	0.46/1		5.71/32	0/0
		3.75/21	0/0		2.14/12	0/0
		1.78/10	0/0	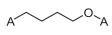	1.61/9	0/0

concentrations. The expression level of ABCB1 in SW620/Ad300 cells remained unchanged when treated with **WS-10** at 20 μM for different time (Fig. 9). This data firmly confirmed that **WS-10** at 20 μM did not affect expression of ABCB1 in SW620/Ad300 cells, and the reversal effect of **WS-10** was not due to the expression changes of ABCB1 in SW620/Ad300 cells.

We next examined whether **WS-10** could change the location of ABCB1 protein via the immunofluorescence assay. As shown in Fig. 10, the incubation of SW620/Ad300 with **WS-10** for 72 h did not alter the location of ABCB1. Thus, these results suggest that the reversal effect of **WS-10** was not attributed to its effect on the localization of the ABCB1 protein.

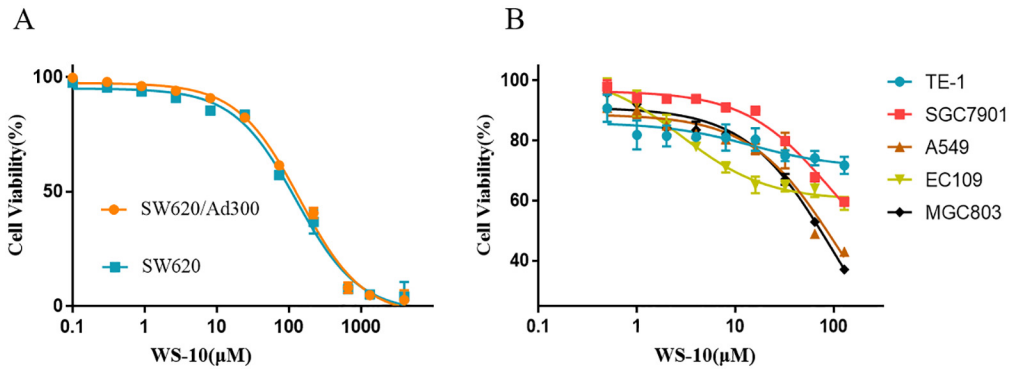

Scheme 1. Synthesis of compound **WS-10**. Reagents and conditions: (a) Na_2CO_3, acetone, 60 °C; (b) Ethyl 3-oxo-3-phenylpropanoate, AcOH, 2 h, reflux.

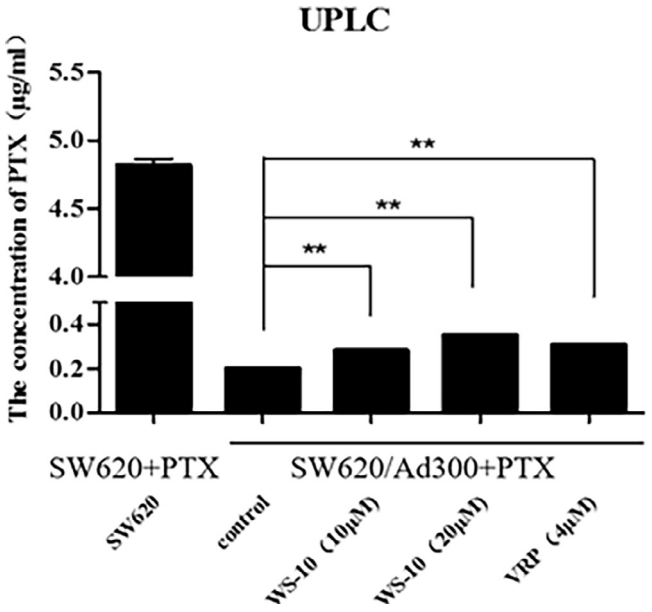

Fig. 4. Cytotoxicity evaluation of **WS-10**. (A) Cytotoxicity of **WS-10** against SW620 and SW620/Ad300 cell lines. (B) Cytotoxicity of **WS-10** against EC109, TE-1, A549, SGC7901, MGC-803 cell lines.

Table 2
Reversal effects of **WS-10** on ABCB1-mediated MDR in SW620 and SW620/Ad300 cell lines.

Treatment	SW620		SW620/Ad300	
	IC_{50} (nM)	RF[a]	IC_{50} (μM)	RF[a]
Paclitaxel	5.29 ± 0.58	1.00	3.39 ± 0.84	642.90
+ **WS-10** (10 μM)	6.32 ± 1.66	1.20	1.47 ± 0.27*	279.20
+ **WS-10** (20 μM)	4.26 ± 0.35	0.81	0.66 ± 0.05**	125.80
+ verapamil (4 μM)	6.79 ± 1.88	1.29	0.83 ± 0.27**	156.74
Doxorubicin	213.18 ± 85.08	1.00	6.15 ± 0.63	28.86
+ **WS-10** (10 μM)	249.10 ± 28.59	1.17	1.28 ± 0.27**	6.02
+ **WS-10** (20 μM)	242.29 ± 34.91	1.14	0.80 ± 0.03**	3.77
+ verapamil (4 μM)	252.55 ± 29.56	1.18	0.92 ± 0.01**	4.32
Cisplatin	1619.77 ± 63.15	1.00	0.61 ± 0.03	0.38
+ **WS-10** (10 μM)	1739.96 ± 53.60	1.07	1.55 ± 0.20	0.96
+ **WS-10** (20 μM)	1576.68 ± 46.38	0.97	1.64 ± 0.01	1.01
+ verapamil (4 μM)	1781.34 ± 233.82	1.10	1.59 ± 0.09	0.98

[a] The resistance fold (RF) values represent the ratios obtained by dividing IC_{50} value of anticancer agents in SW620 and SW620/Ad300 cells with or without reversal agent and the IC_{50} value of the respective anticancer drug in SW620 cells without reversal agent. The cell survival was evaluated by the MTT assay. Verapamil was used as a positive control of ABCB1 inhibitor. $^{*}p < 0.05$, $^{**}p < 0.01$ *versus* that obtained in the absence of inhibitor.

2.7. The CETSA assay for validation of target engagement between *WS-10* and ABCB1

The cellular thermal shift assay (CETSA) is used for the validation of target engagement. Compounds that bind to their target in cells would increase the stability of target protein, which will be detected at higher temperatures. As shown in Fig. 11, **WS-10** stabilized ABCB1 in SW620/Ad300 cells at higher temperatures, showing target engagement of **WS-10** to ABCB1. The results suggest that the binding between **WS-10** and ABCB1 could be, at least in part, responsible for the reversal effect of **WS-10** toward ABCB1-overexpressed cell lines.

2.8. Molecular models of *WS-10* interactions in the inward-occluded and inward-open human ABCB1

To explore the inhibition mechanism of **WS-10**, we docked **WS-10** to different models of ABCB1. Crystallographic and pharmacological data from ABCB1 and other ABC exporters have revealed that these proteins adopt a spectrum of different conformations. During the substrate transport cycle, the inward-open and semi/inward-occluded states have possible portals open to the cytoplasm and the cell membrane for substrate entry,[28] which can be used as the receptor conformation for substrate binding. For years, structures of mouse ABCB1 in the inward-open state have been used to perform molecular docking studies.[29–35] Recently, an human-mouse chimeric ABCB1 in the inward-occluded conformation with an inhibitor binding in a central, enclosed pocket (PDB code: 6FN1) was revealed, and its apo form (PDB code: 6FN4) now hence can be used as the template for homology modeling of inward-occluded human ABCB1.[36] Though a human ABCB1 structure has also been reported,[37] it is not suitable for illustrating the binding site of **WS-10**, because its outward-open conformation represents a posttraslocation state in which the substrate has already been released to the extracellular side of the membrane.

Table 3
Reversal effects of **WS-10** on ABCB1-mediated MDR in HEK293T/NC and HEK293T/ABCB1 cell lines.

Treatment	HEK293T/NC		HEK293T/ABCB1	
	IC_{50} (nM)	RF[a]	IC_{50} (μM)	RF[a]
Paclitaxel	1.93 ± 0.06	1.00	0.09 ± 0.02	47.36
+ **WS-10** (10 μM)	1.67 ± 0.08	0.87	0.05 ± 0.002*	27.80
+ **WS-10** (20 μM)	1.61 ± 0.16	0.83	0.04 ± 0.006*	19.37
+ verapamil (4 μM)	1.62 ± 0.16	0.84	0.03 ± 0.02*	15.69
Doxorubicin (DOX)	71.03 ± 1.39	1.00	1.17 ± 0.09	16.52
+ **WS-10** (10 μM)	80.71 ± 4.73	1.14	0.38 ± 0.02**	5.36
+ **WS-10** (20 μM)	76.61 ± 5.33	1.08	0.29 ± 0.08**	4.05
+ verapamil (4 μM)	75.99 ± 4.67	1.07	0.29 ± 0.04**	4.10
Cisplatin	7840.25 ± 593.42	1.00	7.22 ± 0.45	0.92
+ **WS-10** (10 μM)	8180.24 ± 649.95	1.04	8.26 ± 0.36	1.05
+ **WS-10** (20 μM)	7717.03 ± 446.70	0.98	7.16 ± 0.53	0.91
+ verapamil (4 μM)	6948.72 ± 556.24	0.89	7.10 ± 0.33	0.91

[a] The resistance fold (RF) values represent the ratios obtained by dividing IC_{50} value of anticancer drug in HEK293T and HEK293T/ABCB1 cells with or without reversal agent and the IC_{50} value of the respective anticancer drug in HEK293T cells without reversal agent. The cell survival was evaluated by the MTT assay. Verapamil was used as a positive control of ABCB1 inhibitor. $^{*}p < 0.05$, $^{**}p < 0.01$ *versus* that obtained in the absence of inhibitor.

Thus, **WS-10** was docked to homology models of human ABCB1 in the inward-open conformation as well as in the inward-occluded conformation. **WS-10** was docked to the whole surface of human ABCB1 except the nucleotide-binding domain (NBD). We were surprised to find that **WS-10** could bind to two identical sites (site1 and site2) in both the inward-open and the inward-occluded transporter (Fig. 12). Site1 is located in the internal central cavity and surrounded by hydrophobic residues, which is the common binding site of ligands in complex crystal structures, while site2 is a lower binding site bounded by residues from TM4, TM5, TM8 and TM9, which is near the ligand-binding site on the surface of ABCB1 reported in the QZ-Val co-crystal structure. Though the binding poses of **WS-10** in specific pocket of the two ABCB1 states were much different, which mainly arose from the conformational changes of the transporter, there were common interaction modes for each binding site (Fig. 12). **WS-10** interacted with a range of hydrophobic and aromatic amino acids in site1, such as π-π stackings with F983, F336 and Y310. Except for substantial hydrophobic interactions in site2, the 1*H*-benzo[*d*]imidazol and [1,2,4]triazolo[1,5-*a*] pyrimidin-7(4*H*) -one of **WS-10** could also form polar interactions with hydrophilic resides such as N296, Q773 and K826.

Through molecular docking studies, we found **WS-10** could bind to two identical pockets in two distinct transporter conformations and form extensive hydrophobic interactions in both binding sites, consistent with the popular belief that hydrophobic factor is the most important for inhibitory activity. Szewczyk et al. proposed that ligands

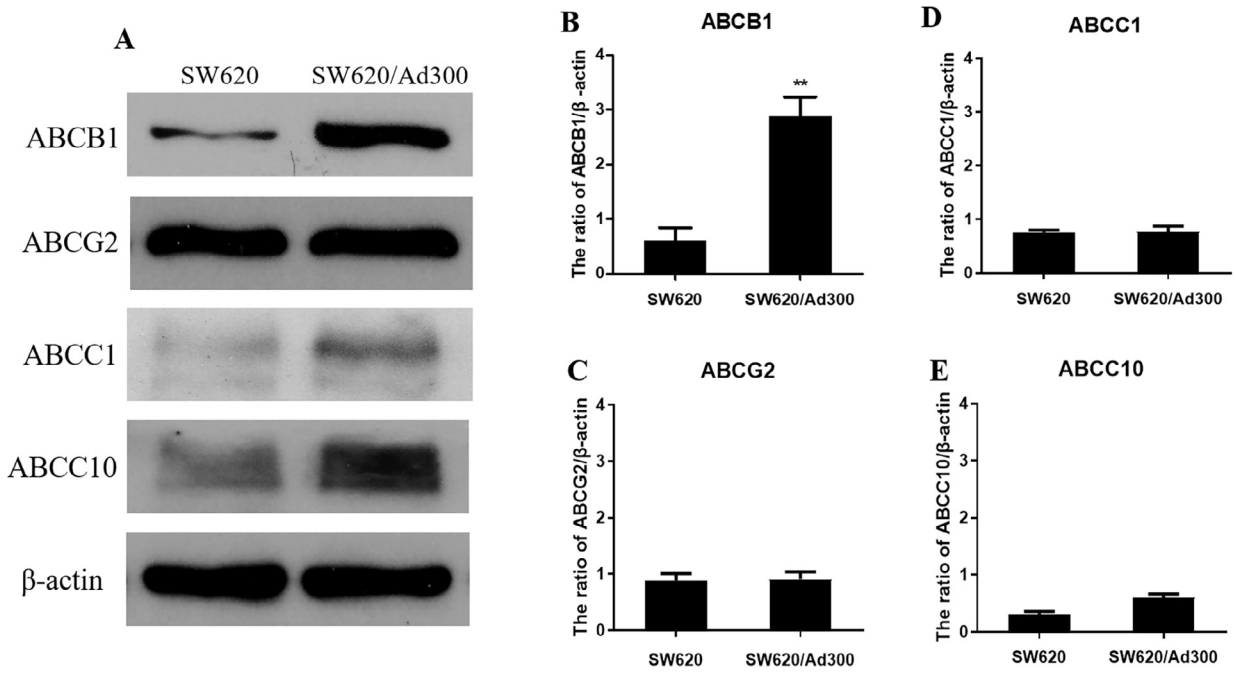

Fig. 5. The effect of **WS-10** on accumulation of paclitaxel. The accumulation of paclitaxel in SW620 and SW620/Ad300 cells with or without **WS-10** treatment. Columns are the mean of triplicate determinations. $^{**}P < 0.01$.

firstly bind near the inner leaflet of the membranes, then move to the central binding cavity. TM4 and TM6 comprise an intramembrane portal for substrate entry.[38] Based on the results of the present study, the site2 seems to be the initial binding site of **WS-10** in ABCB1, and we hypothesize that subsequently **WS-10** translocates to site1 by hydrophobic interactions with the transporter, a process during which large conformational changes occur. However, given the highly dynamic nature of ABCB1, any structure available is only a snapshot in the whole transport cycle, insufficiently to explain a specific binding site. To address this, molecular dynamics simulations are needed to further elucidate the inhibitory mechanism involved in **WS-10**.

3. Conclusions

Because of the prevalence of MDR to chemotherapeutics like paclitaxel and doxorubicin, the identification of new small molecules targeting ABC transporters has been highly pursued in the last few decades. Among these, ABCB1 is the best studied ABC transporter, which plays key roles in the development of multidrug resistance. Therefore, the development of new ABCB1 transporters is needed to overcome ABCB1-mediated MDR. In this work, we first reported the discovery of non-toxic [1,2,4]triazolo[1,5-*a*]pyrimidin-7-one (**WS-10**) from our in-house library that selectively modulates ABCB1-mediated

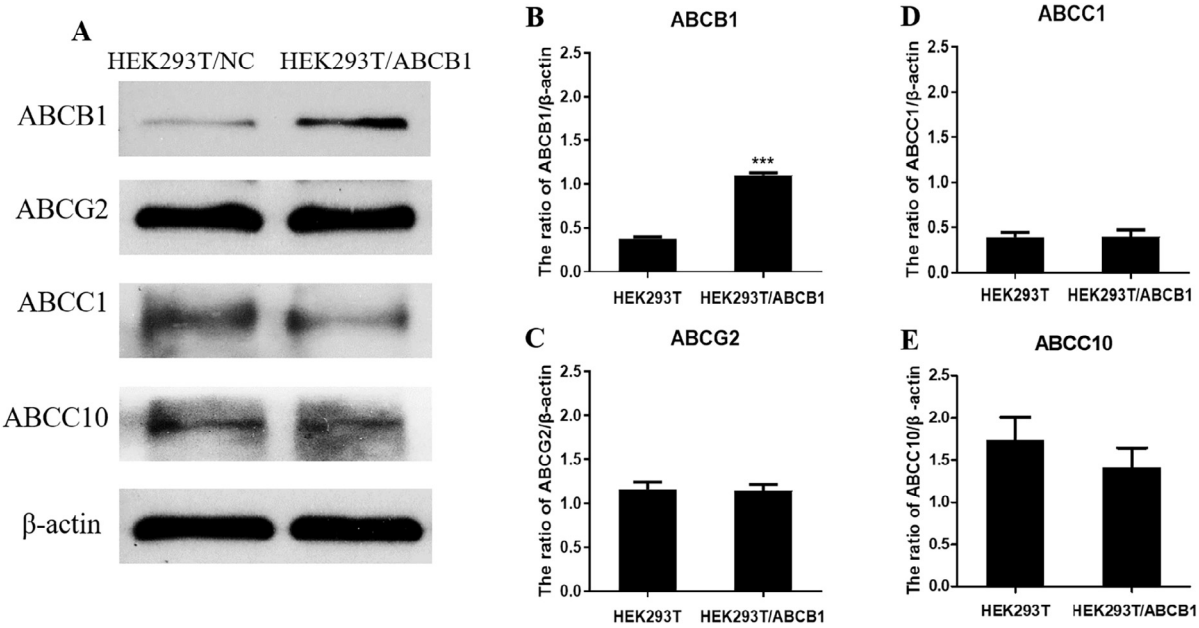

Fig. 6. The protein levels in both SW620 and SW620/Ad300 cells were measured by Western blot analysis. (A) The protein expression of ABCB1, ABCG2, ABCC1, ABCC10 in SW620 and SW620/Ad300 cells; *β*-actin was used as a loading control. (B-E) The gray value analysis of ABCB1, ABCG2, ABCC1, ABCC10, respectively. Values are presented as mean ± SD calculated from three independent experiments. $^{*}P < 0.05$, $^{**}P < 0.01$.

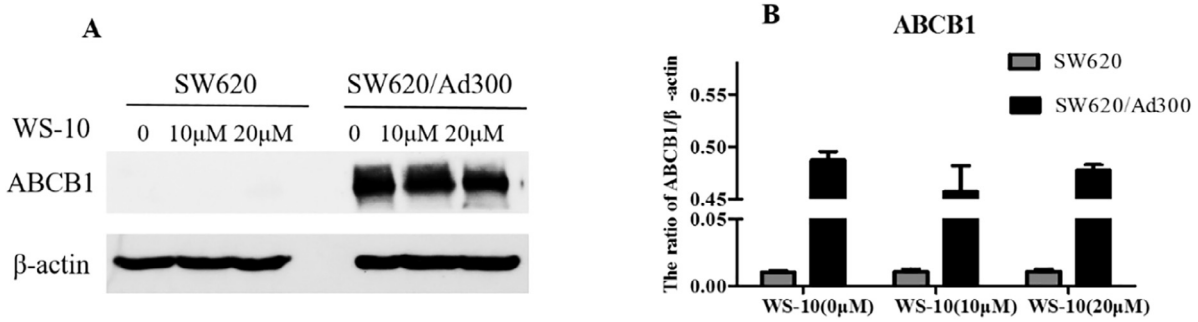

Fig. 7. The protein levels in both HEK293/NC and HEK293/ABCB1 cells were measured by the Western blot analysis. (A) The protein expression of ABCB1, ABCG2, ABCC1, and ABCC10 in HEK293/NC and HEK293/ABCB1 cells; *β*-actin was used as a loading control. (B-E) The gray value analysis of ABCB1, ABCG2, ABCC1, and ABCC10, respectively. Values are presented as mean ± SD calculated from three independent experiments. $^{***}P < 0.001$.

multidrug resistance without affecting expression of other MDR-related proteins ABCB1, ABCG2, ABCC1, and ABCC10. **WS-10** concentration-dependently decreased resistance to paclitaxel and doxorubicin in SW620/Ad300 cells, but showed slightly decreased ABCB1-mediated resistance to doxorubicin in HEK293T/ABCB1 cells. **WS-10** enhanced the intracellular accumulation of paclitaxel in SW620/Ad300 cells, but did not affect the expression of ABCB1 protein and ABCB1 localization. The CETSA assay showed target engagement of **WS-10** to ABCB1, which could be responsible for the reversal effect of **WS-10** toward paclitaxel and doxorubicin in SW620/Ad300 cells. Docking studies showed the possible binding models within ABCB1. Collectively, **WS-10** could be used as a template for designing new nontoxic ABCB1 modulators to overcome ABCB1-mediated multidrug resistance to chemotherapeutics.

4. Experimental section

4.1. General

Reagents and solvents were purchased from commercial sources and were used without further purification. Thin-layer chromatography (TLC) was carried out on glass plates coated with silica gel and visualized by UV light (254 nm). The products were purified by column chromatography over silica gel (200–300 mesh). Melting points were determined on a X-5 micromelting apparatus and are uncorrected. All the NMR spectra were recorded with a Bruker DPX 400 MHz spectrometer with TMS (Tetramethylsilane) as an internal standard in DMSO-d_6. Chemical shifts are given as δ ppm values relative to TMS. High-resolution mass spectra (HRMS) were recorded on a Waters micromass Q-T of micromass spectrometer. Paclitaxel and verapamil were purchased from Meilun Biology Technology Co., Ltd. (Dalian, China). Puromycin was purchased from Solarbio Life Sciences (Beijing, China). The 3-(4,5-Dimethylthiazol-2-yl)-2, 5-diphenyltetrazolium bromide (MTT) and Hoechst 33,342 were obtained from Beyotime Biotechnology (Shanghai, China). The primary antibodies against ABCC10 and ABCG2 were purchased from Abcam (Cambridge, MA, USA). The primary antibodies against ABCB1 and ABCC1 were from Cell Signaling Technology, Inc. (Danvers, MA, USA). The primary antibodies against horseradish peroxidase-labeled anti-mouse IgG and GAPDH were purchased from Zhongshan Golden Bridge (Beijing, China).

4.2. Chemical space analysis

To reflect the representativeness of our compound set, the following three compounds sets were compared: (a) Approved drugs from DrugBank[39] (release date: 2018-04-02): 2009 approved drugs; (b) literature reported ABCB1 inhibitors: 391 inhibitors compounds (with $IC_{50} < 10\,\mu M$) and 254 inactive compounds (with $IC_{50} \geq 10\,\mu M$), downloaded from ChEMBL on 2018-6-4).[40] (c) ChEMBL 24: 1,671,107 compounds. The chemical standardization was processed by MolVS.[41] Molecules with molecular weight (MW) over 800 Da or with less than two carbon atoms were removed. The chemical space analysis and molecular fragment analysis is done mainly by our in-house developed Python library based on RDKit.[42] Molecular descriptors (MW, nHBDon, nHBAcc, nRotB, and TPSA) were calculated by PaDEL-descriptor.[43] LogP values were calculated by XLOGP3.[44] Venn diagrams were used to

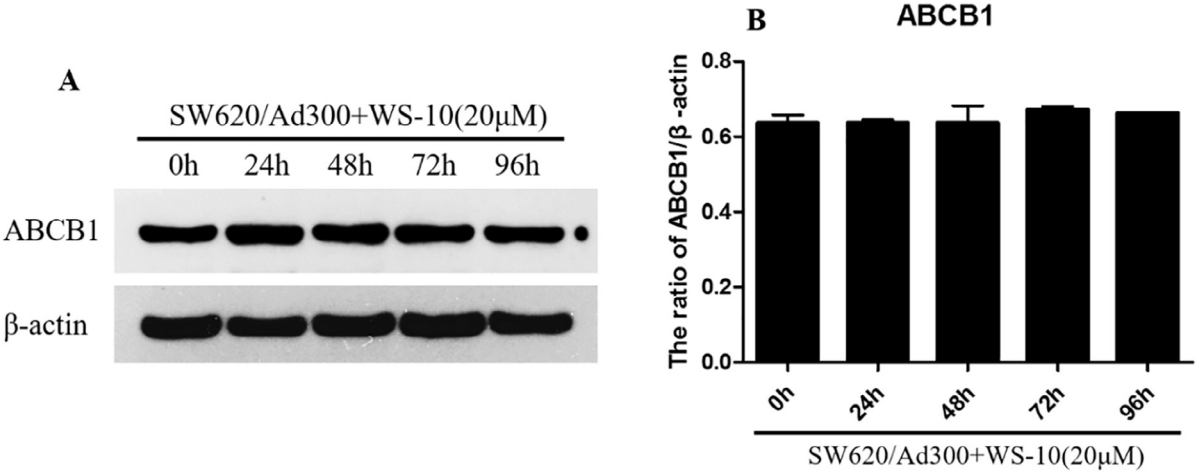

Fig. 8. The expression levels of ABCB1 transporters with different concentrations of **WS-10**. (A) The protein expression of ABCB1 in both SW620 and SW620/Ad300 cells when treated with different concentrations of **WS-10**. The *β*-actin was used as a loading control. (B) The gray value analysis of ABCB1. Values are presented as mean ± SD calculated from three independent experiments.

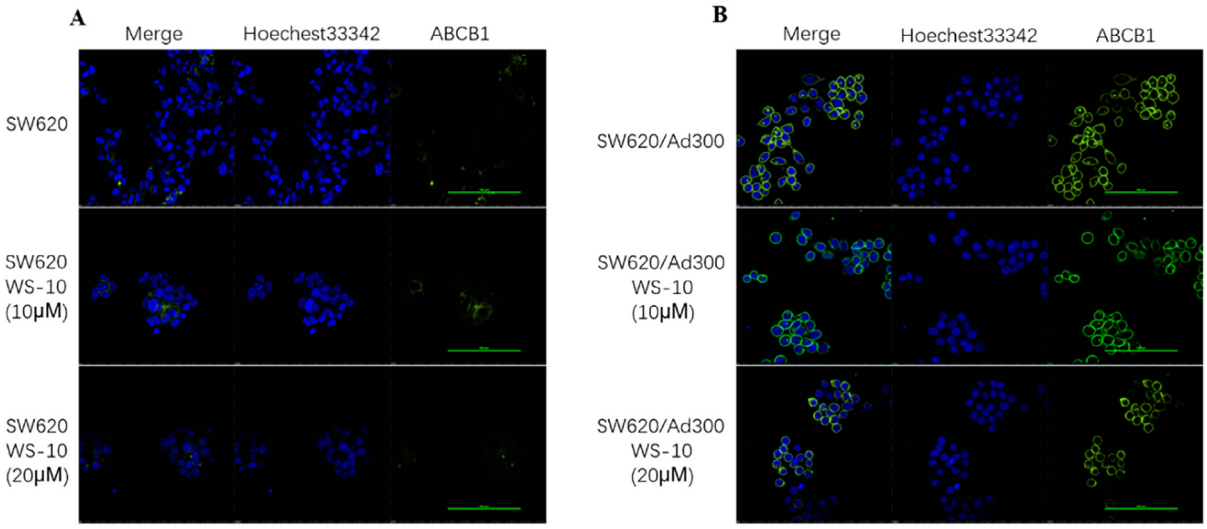

Fig. 9. The expression levels of ABCB1 transporters after treatment with **WS-10** for different time. (A) The protein expression of ABCB1 in SW620/Ad300 cells after treatment with **WS-10** for different time. The *β*-actin was used as a loading control. (B) The gray value analysis of ABCB1. Values are presented as mean ± SD calculated from three independent experiments.

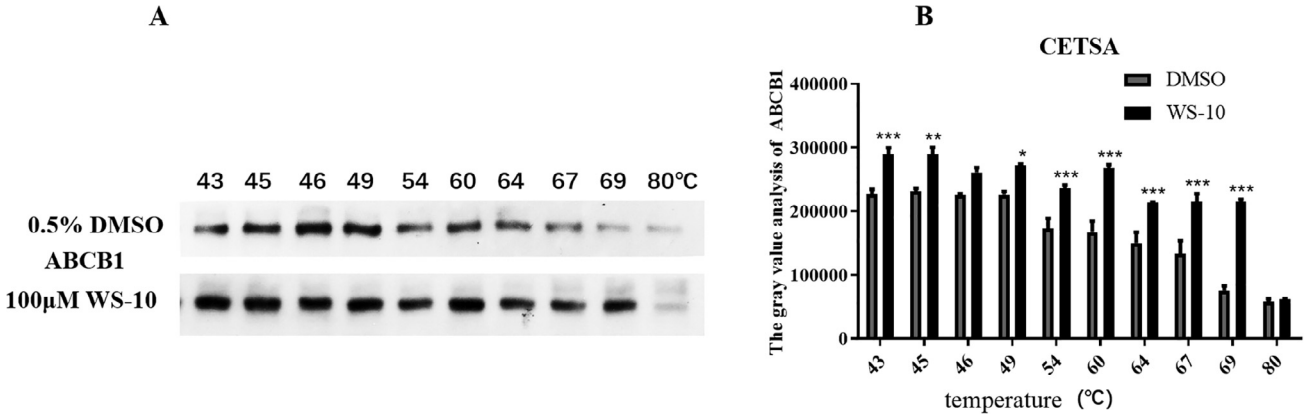

Fig. 10. Effect of **WS-10** on the subcellular localization of ABCB1. (A) Effect of **WS-10** treatment on the subcellular localization of ABCB1 in SW620 cell. (B) Effect of **WS-10** treatment on the subcellular localization of ABCB1 in SW620/Ad300 cells. ABCB1 staining is shown in green. Hoechest33342 (blue) counterstains the nuclei. (For interpretation of the references to color in this figure legend, the reader is referred to the web version of this article.)

depict the intersections of two or more data sets based on InChIKey. Further structural similarity distributions of compound sets were compared based on the maximum pairwise Tanimoto similarities of Morgan fingerprint. To analyze the chemical structural space, Morgan Fingerprint were employed to project all compounds nonlinearly into a 2D similarity space using *t*-Distributed Stochastic Neighbor Embedding (*t*-SNE)[45] by scikit-learn.[46] All Morgan Fingerprint used in this article were based on RDKit function GetMorganFingerprintAsBitVect (radius = 2, nBits = 2048).

4.3. Synthesis of *WS-10* (compound *4*)

4.3.1. Synthesis of compound *3*

To a solution of 3-amino-5-mercapto-1,2,4-triazole (1.0 g) in acetone (30 mL) were added sodium carbonate (1.37 g, 12.92 mmol), sodium iodide (129.06 mg, 0.861 mmol) and 2-(chloromethyl)-1*H*-benzo[*d*]imidazole (1.58 g, 9.47 mmol). The mixture was stirred at 60 °C until the reaction was done. After cooling to room temperature, Na_2CO_3 and NaI were filtered and the residue was concentrated under vacuum and then dissolved with EtOAc. The organic layer was washed with water (2 × 10 mL) and brine (2 × 20 mL) and then dried over $MgSO_4$. After removal of the solvent, the resulting residue was subjected to column chromatography, giving compound **3**, white solid, yield: 60%. ^{1}H NMR (400 MHz, DMSO-d_6) δ 12.30–12.08 (brs, 2H, −N<u>H</u>$_2$), 7.50 (m, 2H, Ar<u>H</u>), 7.25–6.99 (m, 2H, Ar<u>H</u>), 6.14 (s, 2H, N<u>H</u> in triazole and benzimidazole, overlapped), 4.45 (s, 2H, −C<u>H</u>$_2$−). HRMS (ESI): *m/z* calcd for $C_{10}H_9N_6S$ $(M-H)^-$, 245.0609; found, 245.0609.

4.3.2. Synthesis of compound *4*

Compound **3** (1.0 g, 1.0 eq) and benzoylacetic acid ethyl ester (1.0 eq) were dissolved in AcOH (10 mL) and the solution was kept at 120 °C for about 3–6 h. Upon completion of the reaction, the mixture was cooled to room temperature; the white precipitate was filtered, washed with water and dried under vacuum to afford the desired compound **4**. White solid, yield: 35%. m.p.: 256–261 °C. ^{1}H NMR (400 MHz, DMSO-d_6) δ 7.86 (d, J = 6.3 Hz, 2H, Ar<u>H</u>), 7.70–7.46 (m, 5H, Ar<u>H</u>), 7.27 (s, 2H, Ar<u>H</u>), 6.29 (s, 1H, −C<u>H</u>CO−), 4.81 (s, 2H, −SC<u>H</u>$_2$−). ^{13}C NMR (100 MHz, DMSO-d_6) δ 161.28, 155.02, 152.13, 150.94, 150.29, 136.35, 131.93, 131.08, 128.85, 127.46, 122.87, 114.60, 97.40 (−<u>C</u>HCO−), 27.72 (−S<u>C</u>H$_2$−) (*Due to the overlap of aromatic proton signals, some carbon signals are difficult to assign accurately*). HRMS (ESI): *m/z* calcd for $C_{19}H_{13}N_6OS$ $(M-H)^-$, 373.0872; found, 373.0879.

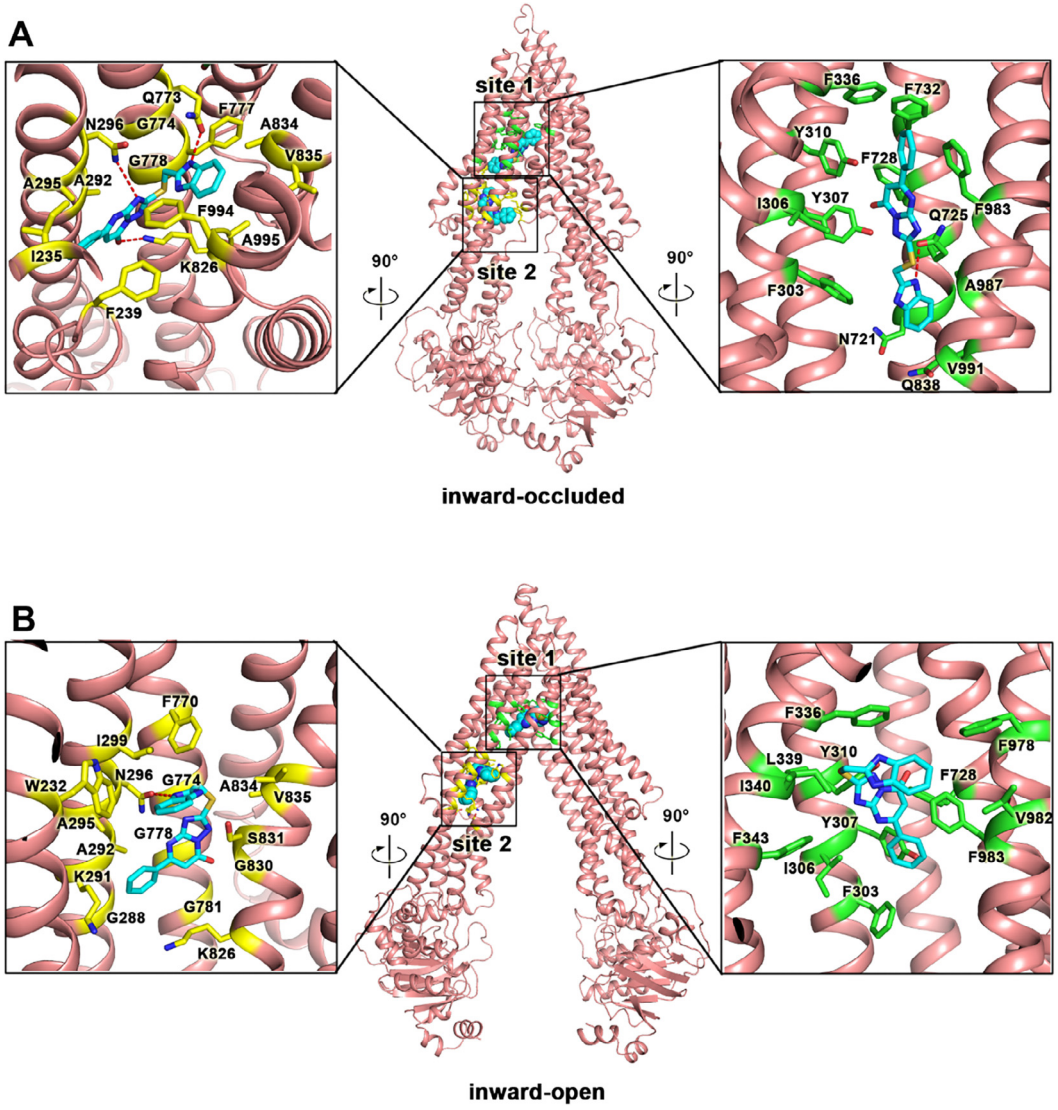

Fig. 11. Target engagement between **WS-10** and ABCB1 in SW620/Ad300 cells. (A) ABCB1 expression levels in SW620/Ad300 cells. (B) The gray value analysis of Western blotting assay. All experiments were performed three times, and data are shown as the mean ± SD from these experiments. $^{*}p < 0.05$, $^{**}p < 0.01$, $^{***}p < 0.005$ *versus* the DMSO control group.

4.4. Cell lines and cell culture

The human colon cancer cell line SW620 and its resistant cell line, SW620/Ad300, were kindly supplied by Dr. Susan Bates's lab (NIH, MD); the human primary embryonic kidney cell line HEK293T's ABCB1 stable gene-transfected cell line HEK293T/ABCB1 and HEK293T/NC were generated by transfecting the HEK293 cells with ABCB1 expression vector or empty vector and were cultured in medium with 1 μg/mL puromycin. All cell lines were maintained in DMEM medium, containing 10% fetal bovine serum and 1% penicillin/streptomycin, and cultured in an incubator at 37 °C with 5% CO_2.

4.5. Cytotoxicity determination by MTT assay[47]

Cells were harvested with trypsin and re-suspended in medium to a final concentration of 7×10^3 cells/mL medium and seeded in 96-well plate. To determine the reversal effect of **WS-10**, different concentrations of the compound (200 μL/well) were added into the wells after

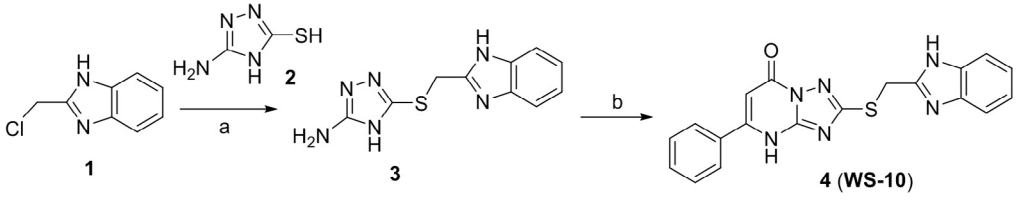

Fig. 12. Overview of the **WS-10** ligand-binding site in human ABCB1 and the detailed interactions. (A) Computational model of interactions between **WS-10** and human-ABCB1 in an inward-occluded conformation. (B) Computational model of interactions between **WS-10** and human-ABCB1 in an inward-open conformation. The transporter (salmon) is shown as cartoon. **WS-10** (cyan) in the middle panel of this picture are shown as spheres for clarify. Residues within 4 Å of **WS-10** as well as **WS-10** itself are depicted in sticks. Hydrogen bonds are shown as red dashed lines. Specific residues in the internal central cavity (binding site1) are colored in green, while residues in site2 are colored in yellow. (For interpretation of the references to color in this figure legend, the reader is referred to the web version of this article.)

incubation at 37 °C for 24 h. After 72 h of incubation at 37 °C, 20 μL MTT solution (5 mg/mL) was added to each well for further incubation at 37 °C for 4 h until dark-blue formazan crystals formed. The medium was discarded, and 150 μL of DMSO was added into each well. Plates were shook to resolve the formazan. Finally, the absorbance was determined at 570 nm by OPSYS microplate reader (Dynex Technologies, Chantilly, VA). The IC_{50} values were calculated by the SPSS software. All experiments were performed three times, and data are shown as the mean ± SD from these experiments.

4.6. Western blot[48]

The cell culture dish was placed in ice and the cells were washed with ice-cold PBS. The PBS was drained; then ice-cold lysis buffer was added. After agitating the cells for 30 min at 4 °C centrifuge in the microcentrifuge at 4 °C, the supernatant was aspirated, placed in a fresh tube kept on ice and concentration of protein was determinate by a BCA Protein Assay Kit (Solarbio Life Sciences, Beijing, China). Equal amounts of total cell lysates were separated using 10% sodium dodecyl sulfate polyacrylamide gel electrophoresis (SDS-PAGE) and transferred into NC membranes through electrophoresis. The NC membranes were blocked in 5% milk in TBST (10 mM Tris–HCl, 150 mM NaCl and 0.1% tween 20) at room temperature for 1 h and then incubated with main antibody at 4 °C overnight. Subsequently, the membranes were washed by TBST and incubated with mouse antibody or rabbit antibody at room temperature for 2 h. Finally, the membranes were washed and the protein–antibody complex was detected by enhanced chemiluminescence detection system.

4.7. Paclitaxel accumulation assay

The accumulation of paclitaxel in SW620/Ad300 or SW620 cells was measured by UPLC.[49] Briefly, the cells (5×10^6 cells) were resuspended and incubated in DMEM medium with the presence or absence of **WS-10** (10 and 20 μM) or verapamil (4 μM) at 37 °C for 72 h. Then the medium was discarded, new medium with the same concentrate (20 μM) of paclitaxel was added at 37 °C for 3 h and subsequently washed twice with ice-cold PBS. Then cells were lysed and resuspended in 1 mL PBS. Paclitaxel was released from the cell by sonication and further extracted with ethyl acetate. The standard curve was done with different concentrations of paclitaxel standard sample (0.031, 0.063, 0.126, 0.252, 0.525, 1.050, 2.100, 4.200, 8.000 μg/mL) by UPLC. The retention time was 1.56 min. Finally, the concentration of paclitaxel was determined with paclitaxel standard curve of UPLC.

4.8. Immunofluorescence analysis[50]

Cells (3×10^4) were seeded in 24-well plates and placed in an incubator overnight, followed by treatment with 10 μM and 20 μM of **WS-10** for 72 h. Then the cells were fixed in 4% paraformaldehyde for 20 min, permeabilized by 0.1% Triton X-100 for 10 min and then blocked with 5% BSA for 1.5 h at room temperature. Subsequently, cells were incubated with primary antibody overnight at 4 °C, followed by Alexa Fluor 488 conjugated secondary antibody (1:800) for 1 h. Then the cells were kept in Hoechst 33,342 (5 μg/mL, Solarbio Life Sciences, Beijing, China) for 20 min at room temperature to counterstain the nuclei. Immunofluorescence images were collected using a laser scanning confocal microscope (Olympus, FV10i, Olympus Corporation, Tokyo, Japan).

4.9. The cellular thermal shift assay[18]

The cells were collected to obtain the total cell lysate, followed by addition of **WS-10** or DMSO into the cell lysate for 30 min. Subsequently, the cells were separated into 11 tubes and then treated at the indicated temperature. Finally, the Western blot was used to detect the quantity of protein.

4.10. Molecular modeling

To investigate the interaction mode between **WS-10** and human ABCB1, molecular docking studies were conducted using AutoDock Tools package (version 1.5.6).[51] Modeling of human ABCB1 in different conformations were performed on the SWISS-MODEL server.[52] The apo form of mouse ABCB1 in the inward-open conformation (PDB code: 4Q9H), which was reported to be able to bind to a series of cyclic peptides such as QZ-Ala (PDB code: 4Q9I), QZ-Val (4Q9J), QZ-Leu (4Q9K) and QZ-Phe (4Q9L),[43] as well as the apo form of human-mouse chimeric ABCB1 in the inward-occluded conformation (PDB code: 6FN4), which could bind to an inhibitor zosuquidar (PDB code: 6FN1),[25] were used as templates for human ABCB1 modeling. The sequence identity of the inward-open model and the inward-occluded model is 88.89% and 91.43%, respectively. The Ramachandran Plots showed that the backbone dihedral angles of 94.69% residues in the inward-open model and 93.47% residues in the inward-occluded model were in energetically favored regions, validating the good quality of both models (Supplementary Figs. S1 and S2). In the docking simulation, **WS-10** was used as a ligand, while human ABCB1 models were used as the receptors. The structure of ABCB1 and **WS-10** were optimized and prepared to the pdbqt format files used for docking by AutoDock Tools. For each model, four grids files with varying xyz-coordinates (152.86/150.93/148.97, 162.86/155.93/168.97, 127.86/150.93/168.97 and 127.86/150.93/148.97) were generated to probe the whole structure of ABCB1 except two ATPase domains. The dimensions of docking grid were 36 Å × 36 Å × 36 Å. All the other parameters were set to the default values. After that, **WS-10** was docked to both models with 20 complexes output per docking run, the results of which were ranked based on the value of their binding energies. The most minimal energy complex was then selected as the reliable binding mode. The results were analyzed and visualized using PyMOL (http://www.pymol.org).

4.11. Statistical analysis

Each experiment was repeated at least three times. All data were presented as the mean ± standard deviation (SD) and analyzed using the SPSS 21.0 software. Statistical analysis was performed by un-paired student *t*-test for comparing two groups in immunoblotting. Statistical significance was set at $p < 0.05$. Statistical analysis was performed using GraphPad Prism version 5.0 for Windows (GraphPad Software, La Jolla, CA).

Acknowledgement

This work was supported by the National Natural Science Foundation of China (No. 81430085, 81773562 and 81703326), Scientific Program of Henan Province (No. 182102310123), China Postdoctoral Science Foundation (No. 2018M630840), the Open Project of Guangdong Provincial Key Laboratory of New Drug Screening (No. GDKLNDS-2018OF006), Key Research Program of Higher Education of Henan Province (No. 18B350009), and the Starting Grant of Zhengzhou University (No. 32210533). We also thank Drs. Susan Bates and Robert Robey (NIH, MD) for their SW620 and SW620/AD300 cell lines.

Appendix A. Supplementary data

Supplementary data associated with this article can be found, in the online version, at https://doi.org/10.1016/j.bmc.2018.08.021.

References

[1]. Dawood S, Leyland-Jones B. Pharmacology and pharmacogenetics of chemotherapeutic agents. *Cancer Invest.* 2009;27:482–488.
[2]. Shustik C, Dalton W, Gros P. P-glycoprotein-mediated multidrug resistance in

tumor cells: biochemistry, clinical relevance and modulation. *Mol Aspects Med.* 1995;16:1–78.
[3]. Quintieri L, Fantin M, Vizler C. Identification of molecular determinants of tumor sensitivity and resistance to anticancer drugs. *Adv Exp Med Biol.* 2007;593:95–104.
[4]. Altenberg GA. Structure of multidrug-resistance proteins of the ATP-binding cassette (ABC) superfamily. *Curr Med Chem Anticancer Agents.* 2004;4:53–62.
[5]. Tiwari AK, Sodani K, Dai CL, Ashby CJ, Chen ZS. Revisiting the ABCs of multidrug resistance in cancer chemotherapy. *Curr Pharm Biotechnol.* 2011;12:570–594.
[6]. Zhang YK, Wang YJ, Gupta P, Chen ZS. Multidrug resistance proteins (MRPs) and cancer therapy. *AAPS J.* 2015;17:802–812.
[7]. Yamaguchi H, Hishinuma T, Endo N, et al. Genetic variation in ABCB1 influences paclitaxel pharmacokinetics in Japanese patients with ovarian cancer. *Int J Gynecol Cancer.* 2006;16:979–985.
[8]. Ferry DR, Russell MA, Cullen MH. P-glycoprotein possesses A 1,4-dihydropyridine-selective drug acceptor site which is allosterically coupled to a vinca-alkaloid-selective binding site. *Biochem Bioph Res Co.* 1992;188:440–445.
[9]. Shukla S, Wu CP, Ambudkar SV. Development of inhibitors of ATP-binding cassette drug transporters: present status and challenges. *Expert Opin Drug Metab Toxicol.* 2008;4:205–223.
[10]. Kathawala RJ, Gupta P, Ashby CR, Chen Z. The modulation of ABC transporter-mediated multidrug resistance in cancer: a review of the past decade. *Drug Resist Update.* 2015;18:1–17.
[11]. Tsuruo T, Iida H, Tsukagoshi S, Sakurai Y. Overcoming of vincristine resistance in P388 leukemia in vivo and in vitro through enhanced cytotoxicity of vincristine and vinblastine by verapamil. *Cancer Res.* 1981;41:1967–1972.
[12]. Kelly RJ, Draper D, Chen CC, et al. A pharmacodynamic study of docetaxel in combination with the P-glycoprotein antagonist tariquidar (XR9576) in patients with lung, ovarian, and cervical cancer. *Clin Cancer Res.* 2011;17:569–580.
[13]. Wilson WH, Jamis-Dow C, Bryant G, et al. Phase I and pharmacokinetic study of the multidrug resistance modulator dexverapamil with EPOCH chemotherapy. *J Clin Oncol.* 1995;13:1985–1994.
[14]. Minderman H, O'Loughlin KL, Pendyala L, Baer MR. VX-710 (biricodar) increases drug retention and enhances chemosensitivity in resistant cells overexpressing P-glycoprotein, multidrug resistance protein, and breast cancer resistance protein. *Clin Cancer Res.* 2004;10:1826–1834.
[15]. Fox E, Bates SE. Tariquidar (XR9576): a P-glycoprotein drug efflux pump inhibitor. *Expert Rev Anticancer Ther.* 2007;7:447–459.
[16]. Luurtsema G, Schuit RC, Klok RP, et al. Evaluation of [11C]laniquidar as a tracer of P-glycoprotein: radiosynthesis and biodistribution in rats. *Nucl Med Biol.* 2009;36:643–649.
[17]. Srinivas NR. Understanding the role of tariquidar, a potent Pgp inhibitor, in combination trials with cytotoxic drugs: what is missing? *Cancer Chemother Pharmacol.* 2016;78:1097–1098.
[18]. Wang B, Zhao B, Chen ZS, et al. Exploration of 1,2,3-triazole-pyrimidine hybrids as potent reversal agents against ABCB1-mediated multidrug resistance. *Eur J Med Chem.* 2018;143:1535–1542.
[19]. Lipinski CA, Lombardo F, Dominy BW, Feeney PJ. Experimental and computational approaches to estimate solubility and permeability in drug discovery and development settings. *Adv Drug Deliv Rev.* 2001;46:3–26.
[20]. Veber DF, Johnson SR, Cheng HY, Smith BR, Ward KW, Kopple KD. Molecular properties that influence the oral bioavailability of drug candidates. *J Med Chem.* 2002;45:2615–2623.
[21]. Rogers D, Hahn M. Extended-connectivity fingerprints. *J Chem Inf Model.* 2010;50:742–754.
[22]. Bemis GW, Murcko MA. The properties of known drugs. 1. Molecular frameworks. *J Med Chem.* 1996;39:2887–2893.
[23]. Lewell XQ, Judd DB, Watson SP, Hann MM. Recap retrosynthetic combinatorial analysis procedure: a powerful new technique for identifying privileged molecular fragments with useful applications in combinatorial chemistry. *J Chem Inf Comput Sci.* 1998;38:511–522.
[24]. Degen J, Wegscheid-Gerlach C, Zaliani A, Rarey M. On the art of compiling and using 'drug-like' chemical fragment spaces. *ChemMedChem.* 2008;3:1503–1507.
[25]. Wang S, Zhao LJ, Zheng YC, et al. Design, synthesis and biological evaluation of [1,2,4]triazolo[1,5-*a*]pyrimidines as potent lysine specific demethylase 1 (LSD1/KDM1A) inhibitors. *Eur J Med Chem.* 2017;125:940–951.
[26]. Stordal B, Hamon M, McEneaney V, et al. Resistance to paclitaxel in a cisplatin-resistant ovarian cancer cell line is mediated by P-glycoprotein. *PLoS ONE.* 2012;7:e40717.
[27]. Yamagishi T, Sahni S, Sharp DM, Arvind A, Jansson PJ, Richardson DR. P-glycoprotein mediates drug resistance via a novel mechanism involving lysosomal sequestration. *J Biol Chem.* 2013;288:31761–31771.
[28]. Subramanian N, Condic-Jurkic K, O'Mara ML. Structural and dynamic perspectives on the promiscuous transport activity of P-glycoprotein. *Neurochem Int.* 2016;98:146–152.
[29]. Patel BA, Abel B, Barbuti AM, et al. Comprehensive synthesis of amino acid-derived thiazole peptidomimetic analogues to understand the enigmatic drug/substrate-binding site of P-glycoprotein. *J Med Chem.* 2018;61:834–864.
[30]. Miyata K, Nakagawa Y, Kimura Y, Ueda K, Akamatsu M. Structure-activity relationships of dibenzoylhydrazines for the inhibition of P-glycoprotein-mediated quinidine transport. *Bioorg Med Chem.* 2016;24:3184–3191.
[31]. Klepsch F, Vasanthanathan P, Ecker GF. Ligand and structure-based classification models for prediction of P-glycoprotein inhibitors. *J Chem Inf Model.* 2014;54:218–229.
[32]. Ferreira RJ, Ferreira MJ, dos Santos DJ. Molecular docking characterizes substrate-binding sites and efflux modulation mechanisms within P-glycoprotein. *J Chem Inf Model.* 2013;53:1747–1760.
[33]. Jara GE, Vera DM, Pierini AB. Binding of modulators to mouse and human multidrug resistance P-glycoprotein. A computational study. *J Mol Graph Model.* 2013;46:10–21.
[34]. Prajapati R, Singh U, Patil A, et al. In silico model for P-glycoprotein substrate prediction: insights from molecular dynamics and in vitro studies. *J Comput Aided Mol Des.* 2013;27:347–363.
[35]. Chufan EE, Kapoor K, Sim HM, et al. Multiple transport-active binding sites are available for a single substrate on human P-glycoprotein (ABCB1). *PLoS ONE.* 2013;8:e82463.
[36]. Alam A, Küng R, Kowal J, et al. Structure of a zosuquidar and UIC2-bound human-mouse chimeric ABCB1. *Proc Natl Acad Sci USA.* 2018;115:E1973–E1982.
[37]. Kim Y, Chen J. Molecular structure of human P-glycoprotein in the ATP-bound, outward-facing conformation. *Science.* 2018;359:915–919.
[38]. Szewczyk P, Tao H, McGrath AP, et al. Snapshots of ligand entry, malleable binding and induced helical movement in P-glycoprotein. *Acta Crystallogr D Biol Crystallogr.* 2015;71:732–741.
[39]. Wishart DS, Feunang YD, Guo AC, et al. DrugBank 5.0: a major update to the DrugBank database for 2018. *Nucleic Acids Res.* 2018;46:D1074–D1082.
[40]. Gaulton A, Hersey A, Nowotka M, et al. The ChEMBL database in 2017. *Nucleic Acids Res.* 2017;45:D945–D954.
[41]. https://github.com/mcs07/MolVS (accessed on May 16, 2018).
[42]. RDKit: Open-source cheminformatics; http://www.rdkit.org (accessed on May 16, 2018).
[43]. Yap CW. PaDEL-descriptor: an open source software to calculate molecular descriptors and fingerprints. *J Comput Chem.* 2011;32:1466–1474.
[44]. Cheng T, Zhao Y, Li X, et al. Computation of octanol-water partition coefficients by guiding an additive model with knowledge. *J Chem Inf Model.* 2007;47:2140–2148.
[45]. Maaten L, Hinton G. Visualizing data using t-SNE. *J Mach Learn Res.* 2008;9:2579–2605.
[46]. Pedregosa F, Varoquaux G, Gramfort A, et al. Scikit-learn: machine learning in Python. *J Mach Learn Res.* 2011;12:2825–2830.
[47]. Yu B, Qi PP, Shi XJ, et al. Efficient synthesis of new antiproliferative steroidal hybrids using the molecular hybridization approach. *Eur J Med Chem.* 2016;117:241–255.
[48]. Shi XJ, Yu B, Wang JW, et al. Structurally novel steroidal spirooxindole by241 potently inhibits tumor growth mainly through ROS-mediated mechanisms. *Sci Rep.* 2016;6:31607.
[49]. Novakova L, Matysova L, Solich P. Advantages of application of UPLC in pharmaceutical analysis. *Talanta.* 2006;68:908–918.
[50]. Fan YF, Zhang W, Zeng L, et al. Dacomitinib antagonizes multidrug resistance (MDR) in cancer cells by inhibiting the efflux activity of ABCB1 and ABCG2 transporters. *Cancer Lett.* 2018;421:186–198.
[51]. Morris GM, Huey R, Lindstrom W, et al. AutoDock4 and AutoDockTools4: automated docking with selective receptor flexibility. *J Comput Chem.* 2009;30:2785–2791.
[52]. Waterhouse AM, Bertoni S, Bienert G, et al. SWISS-MODEL: homology modelling of protein structures and complexes. *Nucleic Acids Res.* 2018;46:W296–W303.